Thermochimica Acta 693 (2020) 178778

Contents lists available at ScienceDirect

Thermochimica Acta

journal homepage: www.elsevier.com/locate/tca

The fusion thermochemistry of rubrene and 9,10-diphenylanthracene between 298 and 650 K: Fast scanning and solution calorimetry

Dmitrii N. Bolmatenkov, Mikhail I. Yagofarov *, Timur A. Mukhametzyanov, Marat A. Ziganshin, Boris N. Solomonov

Department of Physical Chemistry, Kazan Federal University, Kremlevskaya str. 18, 420008 Kazan, Russia

ARTICLE INFO

Keywords:
Heat capacity
Fusion enthalpy
Solution enthalpy
Polycyclic aromatic hydrocarbons
Fast scanning calorimetry

ABSTRACT

The fusion enthalpies and the heat capacities of crystalline, molten, and supercooled liquid rubrene ($T_m = 603$ K) and 9,10-diphenylanthracene ($T_m = 523$ K) were measured using fast scanning calorimetry and conventional DSC. The experimental fusion enthalpies at the melting temperature were corrected to 298.15 K according to Kirchhoff's law of thermochemistry. On the other hand, the fusion enthalpies at 298.15 K were determined from the solution enthalpies of these compounds in benzene, considering "like dissolves like" principle. The fusion enthalpies at 298.15 K obtained using independent methods were in mutual agreement. The heat capacity corrections of the fusion enthalpies of the studied non-planar polycyclic aromatic hydrocarbons to 298.15 K were found to be significantly higher than for planar polyaromatics.

The features of measurement of the heat capacities of organic compounds by fast scanning calorimetry in the temperature range of notable volatility were discussed. The complete absence of the mass losses during heating-cooling cycles was found to be unnecessary condition for accurate heat capacity measurement; tolerable mass losses during the procedure were evaluated.

1. Introduction

The crystal and liquid state isobaric heat capacities as well as fusion enthalpy constitute the basic thermodynamic parameters of individual compounds. The typical applications of fusion enthalpy are calculation of crystallinity degree for amorphous substances [1], selection of phase change materials [2], prediction of solubility [3,4]. The knowledge of crystal and liquid heat capacities in wide temperature range is necessary for adjustment of the enthalpies, entropies and Gibbs energies of fusion to temperatures different from the melting point (T_m), including 298.15 K. This is a necessary milestone for the construction of a self-consistent system of thermodynamic parameters of phase transitions (sublimation, vaporization and fusion) at a common reference temperature (e.g. 298.15 K).

Calculation of the fusion enthalpy below the melting point according to Kirchhoff's thermochemical law requires knowledge of the crystal and liquid heat capacity in the same temperature range. The isobaric heat capacities in crystal and liquid state are usually measured by DSC or adiabatic calorimetry, but the study of supercooled liquid heat capacities is in most cases challenged by the fast crystallization of material. The use of fast scanning calorimetry (FSC), with the scanning rates up to 10^6 K·s^{-1}, enables avoiding crystallization, as well as thermal degradation of a sample during the scan. Recently FSC was intensively used for measuring the heat capacity of supercooled liquids that could not be studied before, including silk fibroin [5], polyvinyl alcohol [6], bulk metallic glasses [7], cytosine [8], amino-acids [9] and other low-molecular-weight-organic compounds [10].

In a series of works [11–13] we demonstrated that the fusion enthalpies of aromatic compounds at 298.15 K can be determined using solution calorimetry, independently of their crystallization tendency. Accordingly, DSC, FSC, and solution calorimetry form a system of complimenting methods for studying the fusion thermochemistry between 298.15 K and T_m [10]. Using the available data on the enthalpies of fusion and solution, as well as the heat capacities of the liquid and solid phases, we found that for many planar aromatic hydrocarbons with T_m up to 700 K the fusion enthalpy temperature corrections to 298.15 K were less than 3 kJ mol^{-1} [11,13,14], in contrast with non-planar aromatic hydrocarbons with similar melting points [10,15]. In the present work we tested this observation on two high-melting non-planar aromatic hydrocarbons, namely, 9,10-diphenylanthracene (DPA, $T_m = 523$

* Corresponding author.
E-mail address: MilYagofarov@kpfu.ru (M.I. Yagofarov).

https://doi.org/10.1016/j.tca.2020.178778
Received 8 May 2020; Received in revised form 2 September 2020; Accepted 4 September 2020
Available online 11 September 2020

K) and 5,6,11,12-tetraphenyltetracene (rubrene, RUB, T_m = 603 K). Observation of the systematic differences in the temperature dependence of the fusion enthalpy for planar and non-planar aromatic compounds is an important step in the development of predictive structure-property schemes.

Investigation of such high-melting compounds is also of interest because direct measurement of the heat capacity of the supercooled liquid down to 298.15 K is impossible due to glass transition. To adjust the fusion enthalpy to 298.15 K, the heat capacity of supercooled liquid must be extrapolated below the glass transition temperature. Comparison of the fusion enthalpies at 298.15 K determined by solution calorimetry and FSC allows checking the validity of the extrapolation.

The study of low-molecular-weight compounds using FSC at high temperatures is challenged by influence of strong evaporation. Generally, evaporation may significantly affect the measured heat flow rate and change the mass of the sample. Previously [10,15,16] we limited the temperature range of study to the region where evaporation cannot be detected during the scan. In this work we attempted to extend the range of temperatures available for the study of the volatile samples on FSC by determining the acceptable mass loss during the experiment, i.e., the highest magnitude of mass-loss which still does not influence the measured heat capacity and its reproducibility.

2. Experimental

2.1. Materials

9,10-Diphenylanthracene (DPA, CAS No. 1499-10-1), 5,6,11,12-tetraphenylnaphthacene (RUB, CAS No. 517-51-1), benzophenone (BZP, CAS No. 119-61-9), indium (In, CAS No. 7440-74-6) and poly-*L*-lactic acid (PLLA, CAS No. 33135-50-1) were of commercial origin with initial mass fraction purities greater than 0.98 (See Table S1 of SI). The same RUB and DPA batches were used as in Ref. [17]. The same BZP batch was used as in Ref. [10]. Prior to the experiments RUB was recrystallized from toluene and dried *in vacuo* at 473 K to remove any traces of solvent. Both purified and unpurified samples of RUB were further studied by FSC and DSC, no differences in melting temperatures, enthalpies, and heat capacities were observed. For both compounds purity was checked by powder X-ray diffraction (PXRD) as described previously [18]. Diffraction patterns are shown on Fig. S1. For DPA several crystal forms are known [19,20]. The obtained diffraction pattern agreed with the data reported for solution-grown crystals [19]. 3 crystal forms of RUB are known [21–23]. The PXRD patterns of RUB before and after recrystallization were the same and agreed with PXRD pattern derived from neutron diffraction data for orthorhombic form [23]. T_m of DPA measured by DSC and FSC (see Table 1) agreed with the literature value of 521 K [24]. For orthorhombic form of RUB T_m of 607 K was previously reported [21]. Suppliers of RUB indicate that T_m is equal to 604 K [25] or in the range of 603–608 K [26]. These values agree with T_m measured in the present work (see Table 1).

The purity of RUB and DPA was additionally analyzed using DSC. The purity of BZP was analyzed using an Agilent 7890 B gas chromatograph (GC) equipped with a flame ionization detector. No impurities greater than 0.1 % were observed.

Table 1
Average experimental fusion and solid-solid transition enthalpies of aromatic compounds measured in this work at 0.1MPa[a].

compound	Transition	$\Delta_{trns}H^A(T_{trns})$ kJ mol^{-1}	T_{trns} K
rubrene	cr ⟶ l	46.6 ± 2.3 (DSC)	603.1 ± 1.0 (DSC)
	cr ⟶ l	46.6 ± 2.5 (FSC)	603.1 ± 1.1 (FSC)
9,10-diphenylanthracene	cr II ⟶ cr I	3.7 ± 0.1 (DSC)	459.4 ± 0.2 (DSC)
	cr I ⟶ l	30.6 ± 0.7 (DSC)	523.3 ± 0.2 (DSC)
	cr I ⟶ l	30.1 ± 1.0 (FSC)	521.3 ± 1.1 (FSC)

[a] Expanded uncertainties (0.95 level of confidence, coverage factor is equal 2.0) include the standard deviations of the mean and the standard calibration uncertainties both multiplied by the coverage factor.

2.2. Differential scanning calorimetry

The specific heat capacities, phase transition enthalpies and temperatures were measured using DSC204 F1 Phoenix differential scanning calorimeter (Netzsch, Germany) as described previously [10,27]. Prior to the experiment, aluminum crucibles were annealed at 200 °C. The samples of the mass between 5 and 20 mg were placed in a 40 μL aluminum crucible with a lid containing 0.5 mm diameter hole. Experiments were performed in a dynamic argon atmosphere (150 ml min^{-1}) at the scanning rate of 10 K min^{-1} during fusion enthalpy measurement and 5 K min^{-1} during heat capacity measurement.

For the fusion enthalpy measurements, 2 samples of DPA and 4 samples of RUB were studied. For each compound 3 heating-cooling cycles from room temperature to T_m + 20 K were carried out. Experimental results from DSC measurements are presented in the Supporting Information (see Table S2). In the case of DPA solid-solid phase transition was observed at 459.4 K. No solid-solid phase transition was observed both on the cooling and the subsequent heating scan. All the melting peaks had the same onsets and areas. In the case of RUB, systematic decrease of the melting temperature after each cycle was observed (*ca.* 1 K), so only the first thermograms were taken into consideration during fusion enthalpy and melting temperature determination. To ensure that decomposition does not influence the fusion enthalpies of the compounds, FSC measurements of the fusion enthalpies were additionally performed (Table S3). The average fusion enthalpies and temperatures measured in this work are provided in Table 1. The reproducibilities of temperature and fusion enthalpy calibration were ±0.2 K and ±1 %, respectively. Hereinafter the reproduibilities correspond to expanded standard deviations (0.95 level of confidence, coverage factor 2.0). These values were included into propagated error of the fusion enthalpy and T_m measurement.

For the heat capacity measurement, 3 samples of RUB and 4 samples of DPA were studied. The procedure of the heat capacity measurement included three steps. Firstly, the baseline for the empty crucibles was determined. Then, using the produced baseline, a standard sample (sapphire) with a weight of 21.05 mg and a sample of the studied compound were sequentially measured in the same crucible. In each case, heating-cooling cycle was repeated three times. The second and the third scans were used for the calculations. The temperature program includes the dynamic segments (between 313 K and 453 K for DPA and between 313 K and 513 K for RUB) and two isothermal segments at the lowest and the highest temperatures of the measurements. For two of the DPA samples the first heating scan was extended to 483 K to obtain the heat capacity of the phase I during the second and third scans. The calculation of the heat capacity was performed using the Netzsch Proteus Thermal Analysis 6.1.0. The results are presented in Tables 2 and 3. The uncertainty of heat flow rate calibration was considered as 1 %.

2.3. Fast scanning calorimetry

The heat capacities of DPA and RUB in molten, supercooled liquid, glassy, and crystal state, as well as the fusion enthalpies and melting temperatures were determined using Mettler Toledo Flash DSC1 [28]. To check the accuracy of the heat capacity measurements up to 650 K, PLLA and In were additionally studied, since for these non-volatile compounds recommended heat capacity values are available in literature [29,30]. To study effect of volatility on the heat capacity measurements, BZP was studied up to 433 K.

Table 2
The heat capacities of supercooled liquid, glassy and crystalline RUB measured by DSC and FSC at 0.1 MPa[a].

T, K	$c_{p,m}$, J K^{-1} mol^{-1}
DSC, cr	
323.0	614.5 ± 18.4
343.0	646.7 ± 19.4
363.0	679.3 ± 20.4
383.0	712.3 ± 21.4
403.0	745.6 ± 22.4
423.0	779.4 ± 23.4
443.0	813.5 ± 24.4
463.0	847.9 ± 25.4
483.0	882.8 ± 26.5
503.0	918.0 ± 27.5
FSC, cr	
323.0	619.5 ± 19.8
343.0	653.8 ± 21.6
363.0	687.3 ± 22.8
383.0	720.0 ± 23.6
403.0	751.9 ± 23.9
423.0	782.9 ± 23.8
443.0	813.1 ± 33.6
463.0	842.4 ± 36.5
483.0	870.8 ± 39.8
503.0	898.3 ± 43.3
523.0	925.0 ± 47.1
543.0	962.0 ± 49.2
563.0	992.6 ± 50.0
FSC, l	
433.0	922.6 ± 42.5
453.0	943.8 ± 42.4
473.0	965.2 ± 42.5
493.0	986.7 ± 42.9
513.0	1008.4 ± 43.7
533.0	1030.3 ± 44.9
553.0	1052.3 ± 46.5
573.0	1074.5 ± 49.5
593.0	1095.7 ± 44.7
613.0	1117.3 ± 46.5
FSC, gl	
323.0	620.0 ± 26.1
343.0	656.7 ± 25.9
363.0	693.5 ± 27.1
383.0	730.6 ± 29.4
403.0	767.9 ± 32.3

[a] Expanded uncertainties (0.95 level of confidence, coverage factor is equal 2.0) include the standard deviations of the mean and the standard calibration uncertainties both multiplied by the coverage factor. Standard uncertainties of pressure and temperature *u(p)* = 5 kPa; *u(T)* in measurements by DSC is 0.1 K; *u(T)* in measurements by FSC is 1 K.

Table 3
The heat capacities of supercooled liquid, molten and crystalline DPA measured by DSC and FSC at 0.1 MPa[a].

T, K	$c_{p,m}$, J K^{-1} mol^{-1}
DSC, cr I [b]	
323.0	418.5 ± 12.6
343.0	440.6 ± 13.2
363.0	462.8 ± 13.9
383.0	485.0 ± 14.6
403.0	507.1 ± 15.2
423.0	529.3 ± 15.9
443.0	551.4 ± 16.5
DSC, cr II [b]	
323.0	411.6 ± 12.3
343.0	433.8 ± 13.2
363.0	457.8 ± 13.7
383.0	480.7 ± 14.4
403.0	503.4 ± 15.1
423.0	526.3 ± 15.8
443.0	549.3 ± 16.5
FSC, cr I [b]	
323.0	420.7 ± 15.4
343.0	442.1 ± 15.2
363.0	463.5 ± 15.1
383.0	485.0 ± 14.9
403.0	506.4 ± 15.8
423.0	527.8 ± 17.2
443.0	549.2 ± 18.7
463.0	570.7 ± 26.3
FSC, l	
363.0	546.3 ± 18.0
383.0	564.8 ± 18.4
403.0	583.3 ± 18.9
423.0	603.3 ± 21.4
443.0	621.6 ± 27.8
463.0	639.8 ± 28.3
483.0	658.0 ± 28.9
503.0	676.2 ± 29.7
523.0	694.4 ± 30.7
543.0	713.8 ± 31.0

[a] Expanded uncertainties (0.95 level of confidence, coverage factor is equal 2.0) include the standard deviations of the mean and the standard calibration uncertainties both multiplied by the coverage factor. *u(p)* = 5 kPa; Standard uncertainties *u(T)* in measurements by DSC is 0.1 K; *u(T)* in measurements by FSC is 1 K.

UFS1 chip sensors were conditioned and corrected according to the manufacturers recommendations, and further calibrated using biphenyl, benzoic acid, and anthracene as temperature standards. In the high temperature region RUB was used for calibration, since its melting point was already determined by DSC. The uncertainty of temperature calibration was equal to 1.0 K. Sample mass for all experiments was in the range of 15−400 ng. The FSC scans were performed in nitrogen atmosphere with a flow rate of 40 mL min^{-1} starting from the temperature of 303 K.

The absolute heat capacities of the samples were measured at the scanning rates of ±1000 K s^{-1} and ±5000 K·s^{-1}. The heat capacities of all compounds (RUB, DPA, BZP, PLLA, In) were determined using symmetry line method (described in Section 3.1). For the samples preliminarily melted on the sensor, the effect of these scanning rates on the measured melting temperature was within the calibration uncertainty. The measurements were performed according to the temperature program shown qualitatively on Fig. 1. Several scans at the same cooling and heating rates were performed, and then the absolute heat capacity was derived from the consecutive cooling and heating scans. Before the experiment samples were heated to T_m + 60 K for a complete melting. Then the liquid state heat capacities were measured up to 623 K for RUB and up to 563 K for DPA at 5000 K·s^{-1}. At 1000 K·s^{-1} the maximum temperatures were 573 K and 473 K, respectively. These temperature

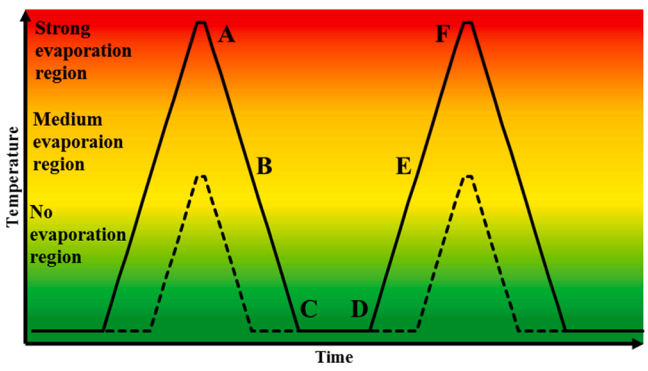

Fig. 1. A temperature program for heat capacity determination by symmetry line method.

ranges were chosen after estimation of the acceptable mass losses (see Section 3.2). In both cases mass loss on heating to these temperatures was less than 2%. Then the samples were crystallized. In the case of RUB, preliminary nucleation at 423 K with subsequent heating to 573 K at 1000 K s^{-1} was necessary to achieve the complete crystallization. In the case of DPA, stochastic cold crystallization occurs on heating around 415 K both at 1000 K s^{-1} and 5000 K s^{-1}. Nonetheless, it was possible to obtain the scans without crystallization at both scanning rates. DPA samples were crystallized completely by heating to 473 K at 1000 K s^{-1}. Crystallization completeness was confirmed by the absence of glass transition around 425 K for RUB and 350 K for DPA and a lack of cold crystallization.

Afterwards, melting of crystallized samples was recorded at 5000 K s^{-1} by heating to T_m + 60 K. For the fusion enthalpy measurement, samples of the masses between 15 and 100 ng were used. The mass loss of both DPA and RUB samples was less than 1 % on heating to T_m + 20 K, so we assumed that the evaporation contribution to the measured heat flow rate increases linearly in the melting temperature range and is a part of the linear baseline for peak integration as in Ref. [8]. The mass loss due to sublimation before melting at the heating rate of 5000 K·s^{-1} was less than 0.2 % and was not considered. Melting peaks of RUB and DPA are shown on Fig. 2. T_m of DPA corresponded to phase I (see Table 1). It is worth noting that on the first heating scan at 5000 K·s^{-1}, T_m of DPA is lower and equals to 511 K, i.e., phase II (metastable above 459 K) is melted.

Amounts of samples were calculated from the absolute heat capacities in crystal state according to Eq. (1) throughout the temperature range of study:

$$n = C_p(\mathrm{cr}, T) / c_{p,m}(\mathrm{cr}, T) \quad (1)$$

(where n is amount of sample, mole; C_p is its absolute heat capacity, J K^{-1}; $c_{p,m}$ is molar heat capacity, J mol^{-1} K^{-1}) using the crystal state molar heat capacity measured by DSC.

5 samples of RUB and DPA, 2 samples of In, 8 samples of PLLA, and 6 samples of BZP were studied; the reproducibility of the heat capacities obtained by FSC was better than ±1%, but the overall error additionally depends on the accuracy of a sample amount determination.

3. Methodology

3.1. Heat capacity determination by fast scanning calorimetry

In the absence of the phase transitions or chemical processes, the heat flow rate after empty sensor subtraction, Φ (W), on cooling and heating can be expressed as:

$$\text{Heating}: \Phi_h(T) = nc_{p,m}(T)\beta_h + \Phi_{HL,h}(T) \quad (2)$$

$$\text{Cooling}: \Phi_c(T) = nc_{p,m}(T)\cdot\beta_c + \Phi_{HL,c}(T) \quad (3)$$

where β (K·s^{-1}) is scanning rate; Φ_{HL} (W) corresponds to heat losses.

If the scanning rates on heating and cooling are the same, then, assuming that $\Phi_{HL,c} = \Phi_{HL,h}$ (*symmetry line*), the sample heat capacity can be calculated as:

$$c_{p,m}(T) = \frac{\Phi_c(T) - \Phi_h(T)}{2\beta\cdot n} \quad (4)$$

An exemplary picture of the heat flow rates and the absolute heat capacities derived using the symmetry line of RUB is provided on Fig. 3.

In Refs. [10,15,16] the agreement in the limits of ±1 % between the heat capacities measured by FSC and the literature values between 200 and 450 K was shown for the low-molecular-weight organic compounds with negligible volatility in this temperature range.

In the present work the heat capacities were measured up to 630 K. Eq. (4) was checked by measuring poly-*L*-lactic acid and indium heat capacities and comparing the results with the critically evaluated literature data [29,30]. For PLLA [29], the measurements accuracy was reported to be better than ±3 %. For In [30], the measurements accuracy was estimated as ±0.3 %.

It was found that the heat flow rate correction, similar with DSC, may be necessary if the studied temperature range is wider.

The comparison of the molar heat capacity of poly-*L*-lactic acid derived from the raw experimental data using the amount determined between 370 and 420 K with the literature [29] is provided on Fig. 4a.

On Fig. 4b the ratios of the measured and literature heat capacities ($c^{app}_{p,m}(T)/c_{p,m}(T)$) of In and PLLA are shown. The amount of In sample was determined in the temperature range 323–393 K. $c_{p,m}(T)$ of In in the temperature range from 400 to 450 K is not provided on Fig. 4b, since its determination by symmetry line method is prevented by melting and crystallization peaks on heating and cooling scans, respectively. In total, 2 In and 8 PLLA samples were studied in the mass range from 40 to 400 ng. The ratios $c^{app}_{p,m}(T)/c_{p,m}(T)$ agreed for all studied samples within the limits of ±1% up to 630 K and varied from 0.93 (630 K) to 1.00 (<450 K). No adjustment is needed below 450 K [10]. The standard deviation of the $c^{app}_{p,m}(T)/c_{p,m}(T)$ ratio for 2 In and 8 PLLA samples is maximal at 630 K, where it is equal to 0.5 %. The averaged ratio $c^{app}_{p,m}(T)/c_{p,m}(T)$ was fitted to cubic polynomial as a function of temperature and was further used for the correction of the heat capacities obtained above 450 K. The details on heat capacity adjustment procedure are provided in Supporting Information.

Secondly, the possible errors due to the non-negligible evaporation of the sample in the measurement range were estimated.

3.2. Establishing of the acceptable mass loss due to evaporation during determination of the heat capacity by symmetry line method

Sample evaporation affects both heating and cooling heat flow rates by changing sample amount n and due to endothermic evaporation effect. Therefore, Eqs. (2 and 3) should be rewritten as:

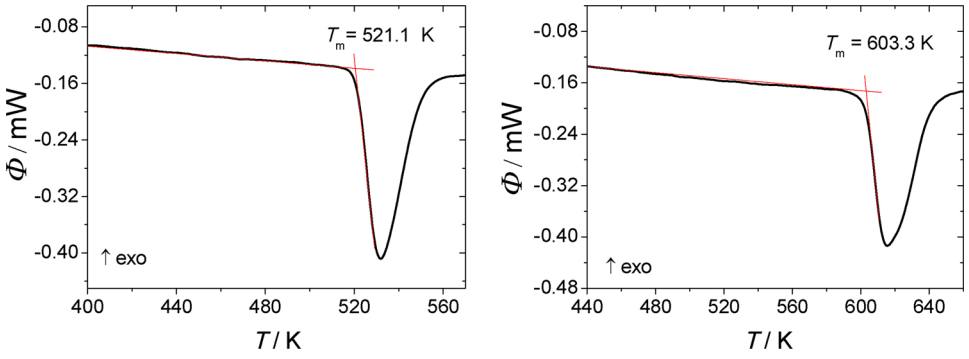

Fig. 2. Melting peaks of DPA (left) and RUB (right) obtained using FSC at the heating rate of 5000 K s^{-1}.

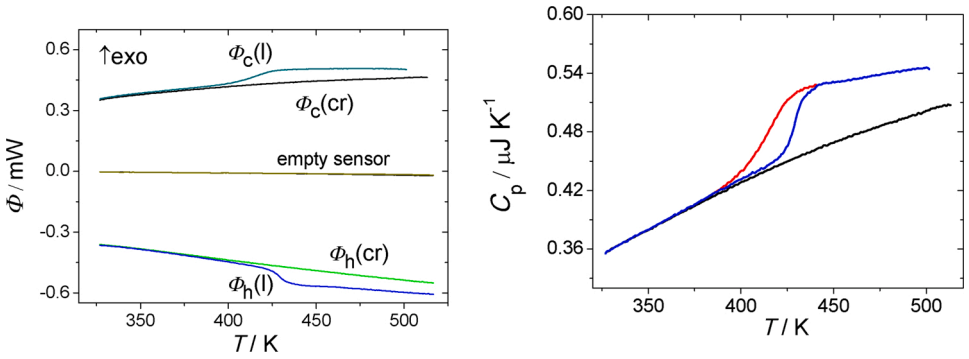

Fig. 3. Heat flows of crystal and liquid RUB and empty sensor recorded at 1000 K s^{-1} (right); the derived crystal (black), supercooled liquid and glassy state (red, from the cooling scan; blue, from the heating scan) absolute heat capacities of RUB. (For interpretation of the references to colour in this figure legend, the reader is referred to the web version of this article).

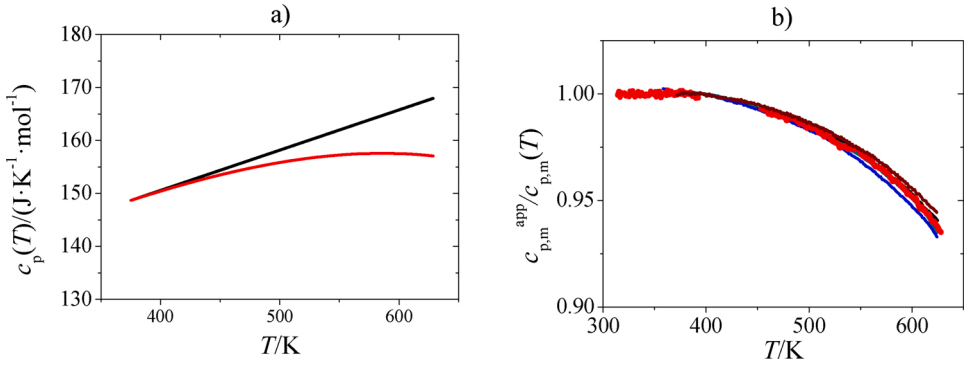

Fig. 4. a) The comparison of the molar heat capacities of poly-*L*-lactic acid measured on Flash DSC (red curve) with the literature data [29] (black curve); b) the ratios of the measured and literature heat capacities as a function of temperature for In sample (solid red line) and 4 PLLA samples (40 ng < m < 400 ng). (For interpretation of the references to colour in this figure legend, the reader is referred to the web version of this article).

$$\Phi_{h/c}(T) = n(T)c_{p,m}(T)\beta_{h/c} + \Phi_{HL}(T) + \\ + \frac{dn}{dt}(T,n)\cdot\Delta^{g}_{cr/l}H(T) \quad (5)$$

where dn/dt (mol/s) is the sample amount loss rate and $\Delta^{g}_{cr/l}H$ is the molar sublimation or vaporization enthalpy. In this work we established what sample amount losses due to evaporation are still acceptable (e.g., the additional heat flow rates affect the measured values by less than ±1%) when applying the symmetry line method for the heat capacity calculation. This was made to extend the temperature range of measurement. The temperature program for heat capacity determination by symmetry line method is qualitatively shown on Fig. 1.

Generally, Eq. (4) may be applied for the temperature program illustrated by the dotted line, where the mass of the sample is the same and the heat flow rate due to evaporation is negligible. Negligibility of the mass loss due to evaporation can be checked by repeated heating and cooling according to this program and comparing the consecutive scans. The systematic decrease of the heat flow rates on cooling and heating indicates evaporation or decomposition. For the majority of the low-molecular-weight organic compounds in FSC experiments evaporation starts at much lower temperatures than decomposition, so we did not further consider decomposition. We analyzed the applicability of Eq. (4) in the region of notable evaporation as follows.

The dependence of the dn/dt on T and n in the stationary conditions may be expressed as [31]:

$$\frac{dn}{dt}(T,n) = Const\cdot S(n)\cdot p(T) \quad (6)$$

where S is evaporation area, p is the vapor pressure of a sample in the layer, and *Const* is the coefficient describing diffusion of the compound to the carrier gas. The latter is only slightly temperature-dependent due to a change in diffusion coefficient, compared to exponential $p(T)$ dependence. Thus dn/dt temperature dependence is mainly determined by the vaporization enthalpy of a compound under study. In this work the latter statement was confirmed by the study of the relation between the mass loss rate of BZP and the temperature (Fig. S4).

On the other hand, the area of liquid droplet on the sensor is proportional to n^k, where $0 < k < 1$ (k depends on the surface tension; it is equal to 2/3 for an ideal semi-sphere). Then, for a particular substance,

$$dn/dt = K\cdot n^k\cdot\exp(-\Delta^{g}_{l}H/(RT)) \quad (7)$$

Evaluation of dn/dt on dynamic segments may be complicated due to the deviation of the vapor pressure over the sample from the equilibrium one. For this reason rate of mass change may be higher on cooling than on heating *ceteris paribus*. However, at heating and cooling rates of 1000 K·s^{-1} these deviations were not detected. Examination of the deviations is described in details in Supporting Information (SI).

It is important to note that one can estimate dn/dt without knowledge of the proportionality coefficient K, but from the decrease of absolute heat capacity of a sample ($nc_{p,m}$) during the consecutive scans. Consider the amount of the sample (Δn) lost during consecutive heating, isotherm at T_{max} (the upper temperature of scan, point A on Fig. 1) of length Δt (s) and cooling. Δn is proportional to the change of the absolute heat capacity of a sample that can be found using Eq. (4) in the temperature range of low volatility (fragment BCDE on the Fig. 1) before and after evaporation. In case of stationary evaporation, the fraction of the sample amount loss (x) at the dynamic segments between temperatures T_0 and T_{max} from the total amount loss Δn is given by Eq. (8) (for details see SI):

$$x = \frac{\frac{2}{\beta}\int_{T_0}^{T_{max}} \exp(-\frac{\Delta_l^g H}{RT})dT}{\frac{2}{\beta}\int_{T_0}^{T_{max}} \exp(-\frac{\Delta_l^g H}{RT})dT + \Delta t \cdot \exp(-\frac{\Delta_l^g H}{RT_{max}})} \quad (8)$$

The x values at different T_{max} and $\Delta_l^g H$ are shown in Table S4. In the experiments with low-molecular-weight organic compounds x is typically between 0.5 and 0.9.

Then, considering that the mass loss during the scan AC-DF is equal to $x\Delta n$, and combining Eqs. (5,7 and 8), one can derive an expression for the heat capacity in the region of significant evaporation:

$$c_{p,m}(T) = \frac{\Phi_c(T,\beta,n) - \Phi_h(T,\beta,n)}{\beta \cdot (2n - x\Delta n)} + \\ + \frac{[n^k - (n - x\Delta n)^k]}{\beta \cdot (2n - x\Delta n)} \cdot K \cdot \exp(-\frac{\Delta_l^g H}{RT}) \cdot \Delta_l^g H \quad (9)$$

where $2n$-$x\Delta n$ is approximately equal to the double amount of the sample in the region BCDE.

Thus, the calculated $c_{p,m}$ is mainly overestimated due to the second term. It can be simplified to $\frac{kx(1-x)\Delta_l^g H}{2\beta\Delta t} \cdot (\frac{\Delta n}{n})^2$ (see SI). Thus, to estimate the relative error of the heat capacity measurement due to evaporation, it is enough to monitor the $\Delta n/n$ value experimentally during consecutive heating and cooling scans of the sample and use the literature or calculated [32–34] vaporization enthalpies values. For k, the highest estimate of 1 may be accepted. If the ratio of term defined by Eq. (10) to expected molar heat capacity $c_{p,m}$ is lower than 0.01, it is possible to neglect its influence. We found that the acceptable relative mass change $\Delta n/n$, at which the error in $c_{p,m}$ is less than 1%, is in the range of 8–10 %, and this fraction is practically independent of the chosen vaporization enthalpies and temperatures. This conclusion was confirmed by measuring the heat capacity of BZP up to 433 K (Fig. S6). The relative deviation in this range did not exceed 0.6 %. In the experiments on RUB and DPA $c_{p,m}$ measurement, the mass loss during heating-cooling cycle was far less (2 %).

This conclusion substantially broadens the temperature range in which the symmetry line method can be used for determination of the heat capacity. It should be noted that the relative amount loss $\Delta n/n$ at certain T_{max} decreases with the increase of the sample mass, so the use of large samples reduces error. Nonetheless, too large samples (more than ca. 1000 ng) should be also avoided because of temperature inhomogeneity and thermal lag.

4. Results and discussion

4.1. Evaluation of the uncertainty of the heat capacities determined by FSC and DSC

The uncertainty of molar heat capacity determined using FSC is affected by two factors:

(1) The uncertainty of the heat flow rate measurements in the temperature range in which $c_{p,m}(T)$ was to be determined.
(2) The uncertainty of the $c_{p,m}(T)$ values obtained by conventional methods (i.e., the reference molar heat capacities), which then determine the uncertainty of the sample amount in FSC experiments.

The relative expanded uncertainties, $U_r(c_{p,m})$, of DSC and FSC measurements were calculated by dividing the expanded uncertainties by $c_{p,m}(T)$ at the average temperature of the range investigated. $U_r(c_{p,m})$ of DSC measurements include the calibration uncertainty (better than ±1 %) and the reproducibility of the measurement.

Total relative expanded uncertainties, $U_{r,tot}(c_{p,m})$, of the molar heat capacities of crystal, liquid and glass determined by FSC were calculated as a sum of $U_r(c_{p,m})$ determined by DSC and $U_r(c_{p,m})$ of FSC measurements. The relative expanded uncertainties of FSC measurements are determined by the reproducibility of the measurements, which is generally within the limits of ±1%, similarly with our previous results [10,15,16], and the uncertainty of the correction procedure (absent below 450 K and less than 1% up to 650 K), which is described in Supporting Information.

In heat capacity integral $\left(\int_{T_m}^{298.15} \Delta_{cr}^{l} c_{cr}^{A}(T)dT\right)$, relative expanded uncertainty was derived by combining the following two factors. Firstly, relative expanded error of FSC measurements was calculated as $\sqrt{(U(c_{p,m}(l,T_{av}))^2 + U(c_{p,m}(cr,T_{av}))^2)}/\Delta_{cr}^{l} c_{p,m}(T_{av})$ from the $c_{p,m}$ values at $T_{av} = (T_m + 298.15\ K)/2$. Then it was summed with $U_r(c_{p,m}(cr))$ obtained by DSC.

The average experimental heat capacities of RUB and DPA measured in this work are provided in Tables 2 and 3 with the expanded uncertainties. $c_{p,m}(T)$ were determined at scanning rates ±1000 and ±5000 K s^{-1}.

4.2. Heat capacities of supercooled liquid, molten, glassy and crystalline RUB studied by FSC and DSC

From DSC measurements, linear temperature dependence for $c_{p,m}$(cr, T) of crystalline RUB was obtained between 323 and 503 K: $c_{p,m}$(cr, T)/(J K^{-1} mol^{-1}) = 67.4 + 1.686 · (T/K) with reproducibility ranging from 0.8 to 3.4 % (coverage factor $k = 2$). We consider the overall uncertainty of the $c_{p,m}$(cr, T) measured by DSC as 3.0 %. The extrapolated $c_{p,m}$(cr, 298.15 K) = 570.1 J K^{-1} mol^{-1}. From the literature the value of 579.5 ± 17.4 J K^{-1} mol^{-1} at 298.15 K is available [35]. These values are in agreement within the limits of experimental errors. We calculated the amounts of each FSC sample from the measured C_p(cr, T) and $c_{p,m}$(cr, T) determined by DSC. C_p(cr, T)/$c_{p,m}$(cr, T) for each sample was constant within the limits of 2% within the temperature range from 323 to 503 K. The average samples amounts in the temperature range from 323 to 503 K were used for the further $c_{p,m}(T)$ calculations. $c_{p,m}$(l, T) and $c_{p,m}$(gl, T) were then derived from these amounts and the corresponding $C_p(T)$. RUB exhibits glass transition at T_g = 428.5 ± 1.2 K (heating rate β_h = 1000 K·s^{-1}; expanded uncertainty (0.95 level of confidence, coverage factor is equal 2.0) includes the standard deviation of the mean and the standard calibration uncertainty of FSC both multiplied by the coverage factor).

$c_{p,m}(T)$ were fitted using the following linear functions:

crystalline RUB (323 < T/K < 563):

$c_{p,m}$/(J K^{-1} mol^{-1}) = 131.9 + 1.528 · (T/K); $U_{r,tot}$ < 5.1 %

glassy RUB (323 < T/K < 403):

$c_{p,m}$/(J K^{-1} mol^{-1}) = 22.5 + 1.848 · (T/K); $U_{r,tot}$ < 4.2 %

supercooled liquid and molten RUB (433 < T/K < 613):

$c_{p,m}$/(J K^{-1} mol^{-1}) = 452.0 + 1.085 · (T/K); $U_{r,tot}$ < 4.6 %

$c_{p,m}(T)$ were determined at scanning rates ±1000 and ±5000 K s^{-1}.

The heat capacities values of RUB at different temperatures are shown in Table 2 and on Fig. 5.

4.3. Heat capacities of supercooled liquid, molten and crystalline DPA studied by FSC and DSC

From DSC measurements, linear temperature dependence for $c_{p,m}(T)$ of DPA in forms cr I (metastable below 459 K) and cr II was obtained

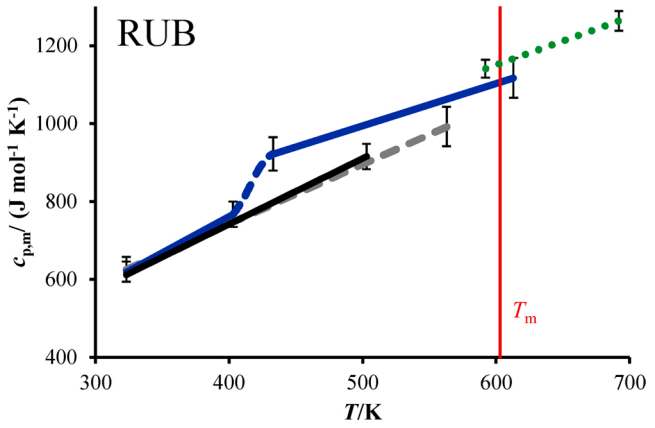

Fig. 5. Heat capacities of supercooled liquid, molten, glassy and crystalline RUB obtained in this work. Solid blue lines – $c_{p,m}$(l, T) and $c_{p,m}$(gl, T) measured by FSC; dashed blue line – region of the glass transition; black solid line – $c_{p,m}$(cr, T) measured by DSC; dashed grey line – $c_{p,m}$(cr, T) measured by FSC; dashed green line – $c_{p,m}$(l, T), *Durupt et al.* [36]. (For interpretation of the references to colour in this figure legend, the reader is referred to the web version of this article).

between 323 and 453 K:

$$c_{p,m}(\text{cr I}, T)/(\text{J K}^{-1}\ \text{mol}^{-1}) = 60.4 + 1.108\ (T/\text{K})$$

$$c_{p,m}(\text{cr II}, T)/(\text{J K}^{-1}\ \text{mol}^{-1}) = 40.8 + 1.148\ (T/\text{K})$$

Reproducibility ranged from 1.0–3.5 % (coverage factor $k = 2$). We consider the overall uncertainty of the $c_{p,m}$(cr, T) measured by DSC as 3.0 %.

We calculated the amounts of each FSC sample from the measured C_p(cr, T) and $c_{p,m}$(cr, T) determined by DSC. C_p(cr, T)/$c_{p,m}$(cr, T) for each sample was constant within the limits of 1% within the temperature range from 323 to 453 K. $c_{p,m}$(l, T) were then derived from these amounts and the corresponding $C_p(T)$. DPA exhibits glass transition at T_g = 342.9 ± 1.2 K (heating rate β_h = 1000 K·s^{-1}; expanded uncertainty (0.95 level of confidence, coverage factor is equal 2.0) includes the standard deviation of the mean and the standard calibration uncertainty of FSC both multiplied by the coverage factor). We do not report $c_{p,m}$(gl, T) values, since the slight increase of the heat capacity due to the glass transition started already at nearly 330 K and below 320 K constant cooling rate of 1000 K·s^{-1} could not be maintained with sensor support temperature of 303 K. At the heating rate of 1000 K·s^{-1} DPA stochastically crystallizes without previous annealing with onset varying from 405 to 415 K.

$c_{p,m}(T)$ were fitted using the following linear functions:

crystalline DPA, cr I (323 < T/K < 473):

$$c_{p,m}/(\text{J K}^{-1}\ \text{mol}^{-1}) = 74.4 + 1.072 \cdot (T/\text{K});\ U_{r,tot} < 4.7\ \%$$

supercooled liquid and molten DPA (363 < T/K < 553):

$$c_{p,m}/(\text{J K}^{-1}\ \text{mol}^{-1}) = 209.8 + 0.928 \cdot (T/\text{K});\ U_{r,tot} < 4.6\ \%$$

The heat capacities values of DPA at different temperatures are shown in Table 3 and on Fig. 6.

[b] cr II is a stable phase up to 459 K; cr I is stable between 459 K and T_m = 523 K and metastable below 459 K.

Durupt et al. [36] reported the equations for the molar heat capacities of liquid DPA ($c_{p,m}/(\text{J K}^{-1}\ \text{mol}^{-1}) = 140.09 + 0.9934 \cdot (T/\text{K})$; 522 K < T < 622 K) and rubrene ($c_{p,m}/(\text{J K}^{-1}\ \text{mol}^{-1}) = 412.01 + 1.2134 \cdot (T/\text{K})$; 592 K < T < 692 K). The measurements were performed using conventional DSC, authors point out the accuracy of ±2 %. The $c_{p,m}$ values in the measurement region predicted by the equations derived in this work agree with the literature in the limits of experimental error.

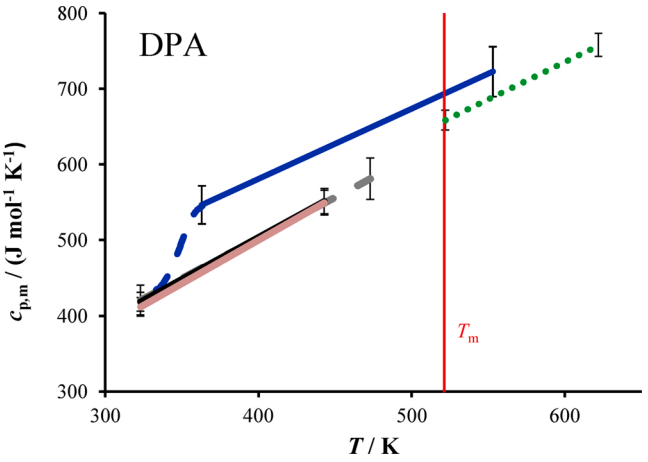

Fig. 6. Heat capacities of supercooled liquid, molten, glassy and crystalline DPA obtained in this work. Solid blue line – $c_{p,m}$(l, T) measured by FSC; dashed blue line – region of the glass transition; black solid line – $c_{p,m}$(cr I, T) measured by DSC; black solid line – $c_{p,m}$(cr I, T) measured by DSC; orange solid line – $c_{p,m}$(cr II, T) measured by DSC; dashed grey line – $c_{p,m}$(cr I, T) measured by FSC; dashed green line – $c_{p,m}$(l, T), *Durupt et al.* [36]. (For interpretation of the references to colour in this figure legend, the reader is referred to the web version of this article).

4.4. Relationships between the enthalpies of solution and fusion of RUB and DPA

Recently we developed the general scheme for the analysis of the relationship between the fusion enthalpy at the melting temperature and the solution enthalpy in benzene at 298.15 K of aromatic compounds [11–13]. According to Hess's law of thermochemistry, the fusion enthalpy of a compound A at 298.15 K ($\Delta^{l}_{cr}H^{A}$ (298.15 K), where A is solid at room temperature) may be expressed as a difference between the solution enthalpy of A at 298.15 K in a solvent S ($\Delta_{soln}H^{A/S}$ (cr, 298.15 K)) and the solution enthalpy of the virtual liquid A at 298.15 K in a solvent S ($\Delta_{soln}H^{A/S}$ (l, 298.15 K)). On the other hand, from Kirchhoff's law of thermochemistry it can be written as a sum of the fusion enthalpy at the melting temperature ($\Delta^{l}_{cr}H^{A}(T_m)$), solid-solid phase transition enthalpies between 298.15 K and T_m ($\sum \Delta_{trns}H^{A}(T_{trns})$), and the heat capacity integral $\left(\int_{T_m}^{298.15} \Delta^{l}_{cr}c^{A}_{p,m}(T)dT\right)$.

$$\begin{aligned}\Delta^{l}_{cr}H^{A}(298.15\text{K}) &= \Delta_{soln}H^{A/S}(\text{cr}, 298.15\text{K}) - \\ &-\Delta_{soln}H^{A/S}(\text{l}, 298.15\text{K}) = \\ &= \Delta^{l}_{cr}H^{A}\left(T_m\right) + \sum \Delta_{trns}H^{A}\left(T_{trns}\right) + \int_{T_m}^{298.15} \Delta^{l}_{cr}c^{A}_{p,m}(T)dT\end{aligned} \quad (10)$$

For solute A and solvent S of a similar structure (e.g., non-self-associated aromatic compound (A) dissolved in benzene (S)), the solution enthalpy of liquid A in S should be close to zero. According to the available experimental data [13], in aromatic compound-benzene systems $\Delta_{soln}H^{A/C_6H_6}$ (l, 298.15 K) is typically in the range 0.8 ± 0.7 kJ mol^{-1}.

The solution enthalpies of RUB and DPA were measured previously [17]: $\Delta_{soln}H^{A/C_6H_6}$ (cr, 298.15 K) for RUB is 10.6 ± 0.2 kJ mol^{-1}; for DPA it is 18.7 ± 0.4 kJ mol^{-1}. According to Eq. (10), the values of the solution enthalpies should be slightly higher (by 0.8 ± 0.7 kJ kJ mol^{-1}) than the fusion enthalpies of DPA and RUB at 298.15 K.

For DPA, the heat capacity integral corresponding to the fusion enthalpy correction from T_m to 298.15 K was $\int_{T_m}^{298.15} \Delta^{l}_{cr}c^{A}_{p,m}(T)dT = -17.9$

$\pm$ 1.1 kJ mol^{-1}. For calculation of the heat capacity integral, $c_{p,m}$(cr II, T) determined by DSC was used below 459 K and $c_{p,m}$(cr I, T) determined by FSC and approximated as a linear function of temperature was used between 459 and 523 K.

$\Delta^{l}_{cr\ I}H^{A}(298.15\ K) = 16.4 \pm 1.2$ of DPA was determined according to Eq. (11) using $\Delta^{cr\ I}_{cr\ II}H^{A}(T_{trns})$ and $\Delta^{l}_{cr\ I}H^{A}(T_{m})$ values determined by DSC.

$$\Delta^{l}_{cr\ II}H^{A}(298.15\ K) = \Delta^{cr\ I}_{cr\ II}H^{A}(T_{trns}) + \Delta^{l}_{cr\ I}H^{A}(T_{m}) + \int_{T_m}^{298.15} \Delta^{l}_{cr}c^{A}_{p,m}(T)dT \quad (11)$$

This value agrees with the solution enthalpy of DPA in benzene.

For RUB, the heat capacity integral corresponding to the fusion enthalpy correction from T_m to 298.15 K was $\int_{T_m}^{298.15} \Delta^{1}_{cr}c^{A}_{p,m}(T)dT = -36.7 \pm 2.5$ kJ mol^{-1}. This value is derived from the liquid and crystal state $c_{p,m}(T)$ measured by FSC. Using the Kirchhoff's law, one can obtain $\Delta^{l}_{cr}H^{A}(298.15\ K) = 9.9 \pm 3.1$ kJ mol^{-1}. Again, an agreement within the limits of experimental error is observed with the solution enthalpy in benzene.

Actually, the $\Delta^{l}_{cr}H^{A}(298.15\ K)$ and $\Delta_{soln}H^{A/C_6H_6}(cr, 298.15K)$ values of the studied non-planar aromatic hydrocarbons at 298.15 K significantly differ from $\Delta^{l}_{cr}H^{A}(T_m)$, as it was also observed previously for 1,3,5-triphenylbenzene and 1,2,3,4-tetraphenylnaphthalene [15]. On the contrary, in Refs [11,13,14]. we shown that for planar aromatic hydrocarbons the difference between the $\Delta_{soln}H^{A/C_6H_6}(cr, 298.15K)$ and $\Delta^{l}_{cr}H^{A}(T_m)$ values is less than 3 kJ mol^{-1} up to T_m = 550 K, e.g. for pyrene (T_m = 423 K), 1,2-benzanthracene (434 K), chrysene (531 K), 1,2,5,6-benzathracene (540 K). For anthracene (489 K) and perylene (551 K) it only slightly exceeds 3 kJ mol^{-1}, compared to the heat capacity integrals found in the present work. Comparison of the fusion enthalpies of planar aromatic hydrocarbons at T_m with the experimental sublimation enthalpies and calculated solvation enthalpies in benzene shows that this remains correct even up to T_m of 700 K, e.g. for benz[*b*]chrysene (574 K), benz[*b*]triphenylene (553 K), benz[*ghi*]perylene (554 K), coronene (710 K) [14]. The reasons of this distinction are to be studied in future research.

5. Conclusions

The theoretical analysis of the contribution of the evaporation into the heat flow rates and the heat capacity obtained by FSC was carried out. The validity of the analysis was confirmed experimentally. This allowed estimating the acceptable mass loss during the cooling-heating cycle in FSC. The performed analysis shows that the acceptable relative mass loss primarily depends on the molar vaporization enthalpy and molar heat capacity of the studied compound. For different compounds these values partially compensate each other, so the acceptable relative mass loss should insignificantly vary with structure. If the mass loss due to evaporation is less than 5 % during heating-cooling cycle, its contribution to the measured heat capacity is usually less than 1%. This notably broadens the range of substances and temperatures appropriate for the heat capacity measurement by FSC.

The fusion enthalpies at T_m, solution enthalpies at 298.15 K, and the heat capacities of crystal and liquid 9,10-diphenylanthracene and rubrene were determined. Their consistency was analyzed based on combined Hess's and Kirchhoff's laws of thermochemistry. The thermochemical values obtained using DSC, FSC, and solution calorimetry agree within the limits of experimental error. It should be mentioned that both compounds have the glass transition temperatures higher than 298 K: 342.9 K (9,10-diphenylanthracene) and 428.5 K (rubrene). Nonetheless, the liquid state heat capacities were treated as linear functions of temperature throughout all the range 298.15 K – T_m. This confirms the previous conclusions based on the analysis of the fusion enthalpies at T_m and the solution enthalpies at 298.15 K: the heat capacities of liquid aromatic compounds between 298.15 K and T_m can be found by linear extrapolation of the heat capacity of the melt.

In this work we observed again that for the studied non-planar polycyclic aromatic hydrocarbons the fusion enthalpy dramatically depends on temperature. At the same time, for the planar polycyclic aromatic hydrocarbons with T_m in the range between 500 and 700 K studied previously the heat capacity integral was substantially smaller. Additional studies are needed for confirmation and explanation of this phenomenon.

CRediT authorship contribution statement

Dmitrii N. Bolmatenkov: Methodology, Investigation, Writing - original draft, Writing - review & editing, Visualization. **Mikhail I. Yagofarov:** Conceptualization, Methodology, Validation, Writing - original draft, Writing - review & editing. **Timur A. Mukhametzyanov:** Writing - review & editing. **Marat A. Ziganshin:** Investigation. **Boris N. Solomonov:** Writing - review & editing, Supervision.

Declaration of Competing Interest

The authors report no declarations of interest.

Acknowledgments

Authors gratefully acknowledge Prof. Christoph Schick for valuable discussion and Mr. Artur E. Boldyrev for assistance with powder X-ray diffraction. The work was funded by the subsidy allocated to Kazan Federal University for the state assignment in the sphere of scientific activities from the Ministry of Science and Higher Education of the Russian Federation, No. 0671-2020-0061.

Appendix A. Supplementary data

Supplementary material related to this article can be found, in the online version, at doi:https://doi.org/10.1016/j.tca.2020.178778.

References

[1] Y. Kong, J. Hay, The measurement of the crystallinity of polymers by DSC, Polymer 43 (2002) 3873–3878.
[2] A. Sharma, V.V. Tyagi, C. Chen, D. Buddhi, Review on thermal energy storage with phase change materials and applications, Renew. Sustain. Energy Rev. 13 (2009) 318–345.
[3] H. Hojjati, S. Rohani, Measurement and prediction of solubility of paracetamol in water− isopropanol solution. Part 2. Prediction, Org. Proc. Res. Dev. 10 (2006) 1110–1118.
[4] C. Held, J. Brinkmann, A.-D. Schröder, M.I. Yagofarov, S.P. Verevkin, Solubility predictions of acetanilide derivatives in water: combining thermochemistry and thermodynamic modeling, Fluid Phase Equilib. 455 (2018) 43–53.
[5] P. Cebe, B.P. Partlow, D.L. Kaplan, A. Wurm, E. Zhuravlev, C. Schick, Using flash DSC for determining the liquid state heat capacity of silk fibroin, Thermochim. Acta 615 (2015) 8–14.
[6] D. Thomas, E. Zhuravlev, A. Wurm, C. Schick, P. Cebe, Fundamental thermal properties of polyvinyl alcohol by fast scanning calorimetry, Polymer (2018).
[7] J.E. Schawe, S. Pogatscher, J.F. Löffler, Thermodynamics of polymorphism in a bulk metallic glass: heat capacity measurements by fast differential scanning calorimetry, Thermochim. Acta 685 (2020), 178518.
[8] A. Abdelaziz, D. Zaitsau, T. Mukhametzyanov, B. Solomonov, P. Cebe, S. Verevkin, C. Schick, Melting temperature and heat of fusion of cytosine revealed from fast scanning calorimetry, Thermochim. Acta 657 (2017) 47–55.
[9] Y.Z. Chua, H.T. Do, C. Schick, D. Zaitsau, C. Held, New experimental melting properties as access for predicting amino-acid solubility, RSC Adv. 8 (2018) 6365–6372.
[10] M.I. Yagofarov, S.E. Lapuk, T.A. Mukhametzyanov, M.A. Ziganshin, C. Schick, B. N. Solomonov, Application of fast scanning calorimetry to the fusion thermochemistry of low-molecular-weight organic compounds: fast-crystallizing m-terphenyl heat capacities in a deeply supercooled liquid state, Thermochim. Acta 668 (2018) 96–102.
[11] M.I. Yagofarov, R.N. Nagrimanov, M.A. Ziganshin, B.N. Solomonov, New aspects of relationship between the enthalpies of fusion of aromatic compounds at the

melting temperatures and the enthalpies of solution in benzene at 298.15 K. Part I, J. Chem. Thermodyn. 116 (2018) 152–158.
[12] M.I. Yagofarov, R.N. Nagrimanov, M.A. Ziganshin, B.N. Solomonov, New aspects of relationship between the enthalpies of fusion of aromatic compounds at the melting temperature and the enthalpies of solution in benzene at 298.15 K. Part II, J. Chem. Thermodyn. 120 (2018) 21–26.
[13] M.I. Yagofarov, R.N. Nagrimanov, B.N. Solomonov, New aspects in the thermochemistry of solid-liquid phase transitions of organic non-electrolytes, J. Mol. Liq. 256 (2018) 58–66.
[14] B.N. Solomonov, M.A. Varfolomeev, R.N. Nagrimanov, T.A. Mukhametzyanov, V. B. Novikov, Enthalpies of solution, enthalpies of fusion and enthalpies of solvation of polyaromatic hydrocarbons: instruments for determination of sublimation enthalpy at 298.15 K, Thermochim. Acta 622 (2015) 107–112.
[15] M.I. Yagofarov, S.E. Lapuk, T.A. Mukhametzyanov, M.A. Ziganshin, C. Schick, B. N. Solomonov, Thermochemical properties of 1, 2, 3, 4-tetraphenylnaphthalene and 1, 3, 5-triphenylbenzene in crystalline and liquid states studied by solution and fast scanning calorimetry, J. Mol. Liq. 278 (2019) 394–400.
[16] M.I. Yagofarov, S.E. Lapuk, T.A. Mukhametzyanov, M.A. Ziganshin, T. F. Valiakhmetov, B.N. Solomonov, The fusion thermochemistry of self-associated aromatic compounds at 298.15 K studied by solution calorimetry, J. Chem. Thermodyn. 137 (2019) 43–47.
[17] B.N. Solomonov, M.A. Varfolomeev, R.N. Nagrimanov, V.B. Novikov, D.H. Zaitsau, S.P. Verevkin, Solution calorimetry as a complementary tool for the determination of enthalpies of vaporization and sublimation of low volatile compounds at 298.15 K, Thermochim. Acta 589 (2014) 164–173.
[18] M.A. Ziganshin, A.V. Gerasimov, S.A. Ziganshina, N.S. Gubina, G.R. Abdullina, A. E. Klimovitskii, V.V. Gorbatchuk, A.A. Bukharaev, Thermally induced diphenylalanine cyclization in solid phase, J. Therm. Anal. Calorim. 125 (2016) 905–912.
[19] J. Adams, S. Ramdas, The crystal structure of solution-grown 9, 10-diphenylanthracene. a combined computational and X-ray study, Acta Crystallogr. B 35 (1979) 679–683.
[20] A.K. Tripathi, M. Heinrich, T. Siegrist, J. Pflaum, Growth and electronic transport in 9, 10-Diphenylanthracene single crystals—an organic semiconductor of high Electron and hole mobility, Adv. Mater. 19 (2007) 2097–2101.
[21] D. Henn, W. Williams, D. Gibbons, Crystallographic data for an orthorhombic form of rubrene, J. Appl. Crystallogr. 4 (1971), 256-256.
[22] L. Huang, Q. Liao, Q. Shi, H. Fu, J. Ma, J. Yao, Rubrene micro-crystals from solution routes: their crystallography, morphology and optical properties, J. Mater. Chem. 20 (2010) 159–166.
[23] M.R.V. Jørgensen, V.R. Hathwar, M. Sist, X. Wang, C.M. Hoffmann, A.L. Briseno, J. Overgaard, B.B. Iversen, Accurate atomic displacement parameters from time-of-flight neutron-diffraction data at TOPAZ, Acta Crystallogr. A 70 (2014) 679–681.
[24] A. Magnus, H. Hartmann, F. Beeker, Verbrennungswärmen und Resonanzenergien von mehrkernigen aromatischen Kohlenwasserstoffen, Z. Phys. Chem. 197 (1951) 75–91.
[25] https://www.fishersci.com/shop/products/5-6-11-12-tetraphenylnaphthacene-purified-by-sublimation-tci-america-2/T2233250MG.
[26] https://www.sigmaaldrich.com/catalog/product/aldrich/554073.
[27] M. Ziganshin, A. Bikmukhametova, A. Gerasimov, V. Gorbatchuk, S. Ziganshina, A. Bukharaev, The effect of substrate and air humidity on morphology of films of L-leucyl-L-leucine dipeptide, Prot. Met. Phys. Chem. Surf. 50 (2014) 49–54.
[28] V. Mathot, M. Pyda, T. Pijpers, G.V. Poel, E. Van de Kerkhof, S. Van Herwaarden, F. Van Herwaarden, A. Leenaers, The Flash DSC 1, a power compensation twin-type, chip-based fast scanning calorimeter (FSC): first findings on polymers, Thermochim. Acta 522 (2011) 36–45.
[29] M. Pyda, R. Bopp, B. Wunderlich, Heat capacity of poly (lactic acid), J. Chem. Thermodyn. 36 (2004) 731–742.
[30] F. Grønvold, Heat capacity of indium from 300 to 1000 K: enthalpy of fusion, J. Therm. Anal. Calorim. 13 (1978) 419–428.
[31] R.N. Nagrimanov, A.A. Samatov, T.M. Nasyrova, A.V. Buzyurov, T. A. Mukhametzyanov, C. Schick, B.N. Solomonov, S.P. Verevkin, Long-chain linear alcohols: reconciliation of phase transition enthalpies, J. Chem. Thermodyn. (2020), 106103.
[32] M.I. Yagofarov, R.N. Nagrimanov, B.N. Solomonov, Relationships between fusion, solution, vaporization and sublimation enthalpies of substituted phenols, J. Chem. Thermodyn. 105 (2017) 50–57.
[33] B.N. Solomonov, M.A. Varfolomeev, R.N. Nagrimanov, V.B. Novikov, A. V. Buzyurov, Y.V. Fedorova, T.A. Mukhametzyanov, New method for determination of vaporization and sublimation enthalpy of aromatic compounds at 298.15 K using solution calorimetry technique and group-additivity scheme, Thermochim. Acta 622 (2015) 88–96.
[34] S. Verevkin, V. Emel'yanenko, V. Diky, C. Muzny, R. Chirico, M. Frenkel, New group-contribution approach to thermochemical properties of organic compounds: hydrocarbons and oxygen-containing compounds, J. Phys. Chem. Ref. Data 42 (2013), 033102.
[35] H. Zhang, J. Brill, Interlayer thermal conductivity of rubrene measured by ac-calorimetry, J. Appl. Phys. 114 (2013), 043508.
[36] N. Durupt, A. Aoulmi, M. Bouroukba, M. Rogalski, Heat capacities of liquid polycyclic aromatic hydrocarbons, Thermochim. Acta 260 (1995) 87–94.